Research Square

Preprints are preliminary reports that have not undergone peer review.
They should not be considered conclusive, used to inform clinical practice,
or referenced by the media as validated information.

Differential Effects of Early-Life Azithromycin and Cefaclor Exposure on Gut Microbiota, Fecal Metabolome, and Body Weight Gain in Juvenile Mice

Yuhui Yao
Department of Pediatrics, The First Hospital of Jiaxing, Affiliated Hospital of Jiaxing University
Shanshan Zhan
Department of Pediatrics, The First Hospital of Jiaxing, Affiliated Hospital of Jiaxing University
Jinhua Hu
Department of Pediatrics, The First Hospital of Jiaxing, Affiliated Hospital of Jiaxing University
Lei Yang
Department of Pediatrics, The First Hospital of Jiaxing, Affiliated Hospital of Jiaxing University
Liang Guo
AI and Omics Research Center,AigenX Biosciences Co., Ltd.
Shunfeng Mao
maoshunfeng@zjxu.edu.cn

Department of Pediatrics, The First Hospital of Jiaxing, Affiliated Hospital of Jiaxing University

Research Article

Keywords: Antibiotics, Gut microbiota, Metabolomics, Early-life exposure, Adiposity

Posted Date: May 24th, 2026

DOI: https://doi.org/10.21203/rs.3.rs-9471199/v1

License: This work is licensed under a Creative Commons Attribution 4.0 International License.
Read Full License

Additional Declarations: No competing interests reported.

Abstract

Background: Early-life antibiotic exposure has been linked to the rising prevalence of childhood obesity. However, the class-specific effects of different antibiotics on host metabolic homeostasis and their distinct mechanisms remain incompletely characterized.

Methods: To elucidate the differential impacts of antibiotics on gut microbiota metabolism, we administered azithromycin (AZM) or cefaclor (CEC) to C57BL/6J mice for four weeks. We monitored body weight change and employed a multi-omics approach combining metagenomic sequencing with LC-MS-based untargeted metabolomics to analyze fecal samples.

Results: We observed that chronic exposure to AZM, but not CEC, was significantly associated with increased body weight gain compared to controls. Shotgun metagenomic analysis revealed that AZM treatment profoundly remodeled the gut microbiota, characterized by an expansion of taxa includi**ng** *Adlercreutzia equolifaciens* and *Enterocloster bolteae*, alongside a marked depletion of the beneficial commensal *Akkermansia muciniphila*. Functionally, the AZM-altered microbiome was enriched in amino acid metabolism pathways. Metabolomic profiling further identified specific perturbations in fecal amino acids (e.g., elevated methionine) and lipid derivatives that were correlated with the observed body weight gain.

Conclusion:

Our findings demonstrate that Early-life high-dose azithromycin, but not standard-dose cefaclor, is associated with increased body weight in juvenile mice. This phenotype coincided with gut microbiota remodeling, enriching *Adlercreutzia equolifaciens* while depleting *Akkermansia muciniphila*, and altered fecal amino acid and lipid metabolites. These findings identify macrolide-associated disruption of the gut microbiota-metabolome axis as a potential mechanism linking early-life antibiotic exposure to weight gain. Further studies employing pharmacokinetically harmonized dosing and causal models are warranted to establish therapeutic relevance.

1. Introduction

Global rates of childhood obesity have climbed steadily over the past five decades, establishing this condition as a dominant pediatric health concern [1]. Beyond its immediate presentation, childhood excess weight predisposes individuals to type 2 diabetes, cardiovascular abnormalities, and metabolic disturbances, while also imposing substantial psychosocial consequences and reduced life quality that commonly extend into adult years [2, 3]. Multiple determinants converge in obesity pathogenesis, including heritable factors, dietary habits, physical activity levels, and environmental conditions. Among modifiable exposures, antibiotic administration during early development has emerged as a putative contributor to subsequent adiposity risk [4–6].

Obesity status correlates consistently with compositional shifts in gut microbial communities [7, 8]. Antibiotic agents themselves do not exert direct adipogenic effects on host tissues. Instead, their primary biological action involves perturbation of the maturing intestinal microbiota during sensitive developmental periods in early life [9]. Such microbial disruption is hypothesized to modify host metabolic signaling and immune function, thereby indirectly fostering conditions permissive for excessive weight accumulation. Critically, animal model experiments and human observational studies demonstrate that antibiotic-induced alterations in microbial community architecture can persist substantially beyond the treatment window, with detectable influences on weight regulation continuing through adolescence and into adulthood [9, 10].

The mechanistic pathways connecting antibiotic-triggered microbiota disruption to altered host energy homeostasis remain inadequately characterized. Additionally, individual antibiotic classes exhibit marked differences in their antimicrobial activity profiles and biological behaviors. Azithromycin (AZM), a representative macrolide, achieves its antibacterial effect through 50S ribosomal subunit binding and consequent inhibition of bacterial protein synthesis, with predominant activity against Gram-positive organisms. Cefaclor (CEC), a second-generation cephalosporin, exerts its action through interference with bacterial cell wall assembly, primarily affecting Gram-negative species. These pharmacological distinctions raise the likelihood that different antibiotic classes may produce divergent consequences for gut microbial ecology and, by extension, host metabolic outcomes.

Children receive antibiotic therapy frequently for routine infections, including acute otitis media, upper respiratory tract infections, and dermatological conditions. Considering this high exposure prevalence alongside escalating childhood obesity rates, investigations examining class-specific antibiotic effects on intestinal microbiota and host metabolism represent a pressing research priority. Direct comparative studies evaluating how distinct antibiotic classes reshape gut microbial composition and metabolic function remain sparse.

This investigation sought to compare associations between early-life exposure to two widely used pediatric antibiotics, azithromycin (AZM, a macrolide) and cefaclor (CEC, a second-generation cephalosporin), and alterations in the gut metagenome and fecal metabolome of juvenile mice. A secondary objective involved identifying microbial and metabolic features correlating with antibiotic-associated body weight changes. This work constitutes an exploratory, hypothesis-generating analysis intended to inform subsequent causal investigations incorporating pharmacokinetically matched dosing regimens, fecal microbiota transplantation approaches, and comprehensive metabolic phenotyping strategies.

2. Materials and Methods

2.1 Animals and Experimental Design

This study was approved by the Animal Care and Use Committee of The First Hospital of Jiaxing, Affiliated Hospital of Jiaxing University (approval number: JXYY2023-027), and all animal experiments were performed in accordance with the National Guidelines for the Care and Use of Laboratory Animals of China and the ARRIVE guidelines. Male C57BL/6J mice (2 weeks old, n = 30) were purchased from Charles River Laboratories and housed in a regulated barrier system facility at 23 – 24°C with 60% ±10% relative humidity and a 12 h light/dark cycle. All of the mice were fed a standard chow diet. The animals had free access to water and food. After a 7-day acclimation period, mice were randomly assigned to 3 groups (n = 10 per group): AZM group (100 mg/kg body weight AZM via daily intragastric gavage for 4 weeks), CEC group (20 mg/kg body weight CEC via daily intragastric gavage for 4 weeks), and Control group (equal volume of vehicle via daily intragastric gavage for 4 weeks). Body weight was measured weekly. Finally, fecal samples were collected for metagenomic sequencing and LC-MS-based untargeted metabolomics (Fig. 1A).

2.2 Fecal Metagenomic Analysis

2.2.1 Sample Testing

DNA was extracted from fecal samples using the CTAB method. Fecal samples were added to 2.0 mL tubes containing 1000 µL CTAB lysis buffer and lysozyme, followed by incubation at 65°C with periodic inversion. The supernatant was collected after centrifugation and mixed with phenol:chloroform: isoamyl alcohol (25:24:1, pH 8.0), then centrifuged at 12,000 rpm for 10 min. The aqueous phase was further purified using chloroform: isoamyl alcohol (24:1) under the same centrifugal conditions. DNA was precipitated with isopropanol at -20°C, then centrifuged (12,000 rpm, 10 min) and washed twice with 75% ethanol. The resulting pellet was air-dried and resuspended in ddH_2O, with an optional 10-min incubation at 55–60°C to facilitate recovery. Finally, residual RNA was removed by adding 1 µL RNase A and incubating at 37°C for 15 min. DNA degradation degree, potential contamination, and DNA concentration were measured using Agilent 2100.

2.2.2 Library Construction

Sequencing library was generated using NEBNext® UltraTM DNA Library Prep Kit for Illumina (NEB, USA, Catalog: E7370L) following manufacturer's recommendations, and index codes were added to each sample. Briefly, the genomic DNA sample was fragmented by sonication to a size of 350 bp. Then DNA fragments were end-polished, A-tailed, and ligated with the full-length adapter for Illumina sequencing, followed by further PCR amplification. After PCR products were purified by the AMPure XP system (Beverly, USA). Subsequently, library quality was assessed on the Agilent 5400 system(Agilent, USA) and quantified by QPCR (1.5 nM).

2.2.3 Sequencing

The qualified libraries were pooled and sequenced on Illumina platforms with a PE150 strategy, according to effective library concentration and data amount required.

2.2.4 Bioinformatics Analysis

2.2.4.1 Data Quality Control and Removal of Host Sequences

The Raw Data of bacteria, fungi and viruses in fecal samples were obtained by metagenomic sequencing using the Illumina Novaseq high-throughput sequencing platform. In order to ensure the reliability of data, the Raw sequencing data needs to be preprocessed using the Kneaddata software. The specific processing steps are as follows: Raw sequencing data were preprocessed using Kneaddata software integrated with Trimmomatic to remove sequencing adapters (parameter: ILLUMINACLIP: adapters_path: 2:30:10) and low-quality bases (parameter: SLIDINGWINDOW: 4:20 with default quality threshold ≤ 20), while eliminating sequences with final length less than 50 bp (parameter: MINLEN:50). To exclude potential host contamination, clean data were aligned to the host reference database using Bowtie2 (http://bowtie-bio.sourceforge.net/bowtie2/index.shtml) with the very-sensitive parameter to filter reads of host origin from subsequent analysis. Finally, the rationality and effectiveness of quality control were assessed using FastQC [11–13].

2.2.4.2 Taxonomy Annotation

Kraken2 and the self-build microbial database (Sequences belonging to bacteria, fungi, archaea, and viruses were screened from the NT nucleic acid database and RefSeq whole genome database of NCBI) were used to identify the species contained in the samples, and then Bracken was used to predict the actual relative abundance of species in the samples. Kraken2 is the latest comparison software based on k-mers. The local Kraken2 database we used contained 16799 known bacterial genomes [14–17].

2.2.4.3 Common Functional Database Annotations Based on Reads

The clean reads after quality control and de-host were used to blast to the database (Uniref90) using Humann2 software (based on Diamond), and the annotation information and relative abundance table from each functional database were obtained according to the corresponding relationship between Uniref90 ID and each database [18–21].

Based on the species abundance table and functional abundance table, abundance clustering analysis, PCOA, NMDS dimension reduction analysis (species only), and sample clustering analysis can be performed. When grouping information is available, Lefse Biomarker and Dunn's test can be performed to excavate differences in species composition and functional composition between samples [22].

2.2.4.4 Antibiotic Resistance Gene Annotation

DIAMOND software [23] was used to align and annotate the quality-controlled, host-depleted clean reads against the Comprehensive Antibiotic Resistance Database (CARD). The alignment parameters were set

as follows: e-value < 1e-3 and percent identity > 80%. The relative abundance of potential antibiotic resistance genes in each sample was subsequently quantified.

2.3 Fecal Untargeted Metabolomics Analysis

2.3.1 Metabolites Extraction

Fecal samples (about 50 mg) were individually ground with liquid nitrogen, and the homogenate was resuspended with prechilled 80% methanol by vortexing. The samples were incubated on ice for 5 min and then centrifuged at 15,000 g, 4°C for 20 min. Some of the supernatant was diluted to a final concentration containing 53% methanol by LC-MS grade water. The samples were subsequently transferred to a fresh Eppendorf tube and then centrifuged at 15000 g, 4°C for 20 min. Finally, the supernatant was injected into the LC-MS/MS system for analysis [24].

2.3.2 UHPLC-MS/MS Analysis

UHPLC-MS/MS analyses were performed using a Vanquish UHPLC system (ThermoFisher, Germany) coupled with an Orbitrap Q ExactiveTM HF mass spectrometer or Orbitrap Q ExactiveTM HF-X mass spectrometer (Thermo Fisher, Germany). Samples were injected onto a Hypersil Gold column (100×2.1 mm, 1.9μm) using a 12-min linear gradient at a flow rate of 0.2 mL/min. The eluents for the positive and negative polarity modes were eluent A (0.1% FA in Water) and eluent B (Methanol). The solvent gradient was set as follows: 2% B (0–1.5 min); linear gradient from 2% to 85% B (1.5–4.5 min); linear gradient from 85% to 100% B (4.5–10.0 min); hold at 100% B (10.0–10.5 min); rapid return to 2% B (10.5–10.6 min); and column re-equilibration at 2% B (10.6–12.0 min). The Q ExactiveTM HF mass spectrometer was operated in positive/negative polarity mode with spray voltage of 3.5 kV, capillary temperature of 320°C, sheath gas flow rate of 35 psi, and aux gas flow rate of 10 L/min, S-lens RF level of 60, Aux gas heater temperature of 350°C.

2.3.3 Data Processing and Metabolite Identification

The data files generated by UHPLC-MS/MS were processed using XCMS for peak alignment, peak picking, and quantitation for each metabolite. Peak intensities were normalized to the total spectral intensity (total ion current) of each sample to correct for technical variation. Pooled quality control (QC) samples were analyzed every 10 injections to monitor instrument stability and metabolite retention time consistency.

2.3.4 Data Analysis

These metabolites were annotated using the KEGG database (https://www.genome.jp/kegg/pathway.html), HMDB database (https://hmdb.ca/ metabolites), and LIPIDMaps database (http://www.lipidmaps.org/).

2.4 Integrated Analysis

2.4.1 Data Preprocessing

Metabolomic abundance matrices were subjected to sample-wise normalization (using median or total sum scaling to correct for library size variations), followed by log transformation to improve normality and feature-wise scaling (Z-score normalization) to ensure equal weighting of variables. Concurrently, metagenomic relative abundance data underwent Hellinger transformation to mitigate the influence of high-abundance taxa and data sparsity.

2.4.2 Correlation and Discordance Analysis

The spatial concordance and explanatory power between the metabolome and metagenome were evaluated using non-supervised models, including Procrustes analysis, Redundancy Analysis (RDA), or Canonical Correspondence Analysis (CCA). Specific interaction patterns were identified via Spearman or Pearson correlation coefficients to construct association heatmaps and interaction networks.

2.4.3 Predictive Modeling and Feature Selection

Supervised machine learning algorithms, specifically Random Forest (RF) and Support Vector Machines (SVM), were employed to identify key biological discriminants. Model robustness and predictive performance were validated using the Receiver Operating Characteristic (ROC) curve analysis.

2.4.4 Functional Enrichment and Integration

To enable a systemic interpretation of the "microbiome-function-metabolome" axis, joint enrichment analyses were performed using Gene Set Enrichment Analysis (GSEA) or Over-representation Analysis (ORA). Differentially abundant taxa and metabolites were mapped onto KEGG pathways to identify coordinated biological shifts.

2.5 Statistical Analysis

Results throughout the manuscript are presented as mean values with their associated standard errors (mean ± SEM). GraphPad Prism version 9 (GraphPad Software, San Diego, CA, USA) was employed for all statistical computations. Between-group comparisons for three independent groups were conducted using one-way analysis of variance (ANOVA); when the overall F-test reached statistical significance, Tukey's honestly significant difference (HSD) test was subsequently applied for pairwise post-hoc analyses. For datasets violating normality assumptions, the Kruskal-Wallis non-parametric test was used, with Dunn's procedure for post-hoc comparisons. Differential abundance testing in multi-omics datasets incorporated false discovery rate (FDR) correction to account for multiple hypothesis testing. Thresholds for statistical significance were set as follows: $*P < 0.05$, $**P < 0.01$, $***P < 0.001$, and $****P < 0.0001$.

3. Results

3.1 Azithromycin Exposure Induces Weight Gain in Juvenile Mice

Body weight trajectories were tracked weekly across the four-week intervention period to assess antibiotic-associated effects on growth. Mice receiving azithromycin (AZM) displayed consistently higher body weights compared to controls beginning at week 2 and continuing through study completion. In contrast, the cefaclor (CEC) group exhibited a weight gain profile statistically indistinguishable from control animals throughout the treatment window (Fig. 1B, 1C). These observations support a positive correlation between AZM exposure and elevated body weight gain in juvenile mice under the conditions tested.

3.2 Antibiotics Influenced Gut Microbiota Composition in Juvenile Mice

To evaluate the impacts of antibiotics on the composition and structure of the intestinal microbiota, we performed metagenomic sequencing analysis on fecal samples from AZM, CEC, and Control groups. Venn diagram analysis identified 444, 138, and 199 unique annotated bacterial species in the AZM, CEC, and Control groups, respectively, with 425 bacterial species shared across all three groups (Fig. 2A). A Principal Coordinates Analysis (PCoA) was performed to investigate the extent of **similarity** of the microbial communities **a**mong the three groups based on Bray-Curtis distance metrics. The analysis indicated that the microbiota composition of the AZM group was significantly different from that of the CEC and Control groups (Fig. 2B). Beta-diversity analysis was visualized based on Non-Metric Multi-Dimensional Scaling (NMDS), which is non-linear and can better reflect the non-linear structure of ecological data and measure differences between groups (Fig. 2C). We found that the microbial composition of the AZM group diverged significantly from both the CEC and Control groups, confirming that antibiotic type is a primary driver of community structure. Subsequently, we evaluated the major taxa distribution and relative abundances (the top 20 of the mean abundance) at the phylum, genus, and species levels.

Phylum-level taxonomic profiling revealed marked compositional differences among treatment groups. Relative to controls, AZM-treated mice showed significant enrichment of *Bacillota* and *Actinomycetota*, whereas both CEC-treated and control animals maintained higher relative abundances of *Verrucomicrobiota* and *Bacteroidota* (Fig. 2D, 2E). Linear discriminant analysis effect size (LEfSe) applied to phylum-level data confirmed these distribution patterns at a threshold of LDA score > 2 (Fig. 2F), indicating that antibiotic class rather than treatment duration per se drove the observed taxonomic shifts.

Rank-ordering the 20 most abundant bacterial genera across all fecal samples uncovered distinct compositional patterns associated with antibiotic treatment. Individual sample profiles (Fig. 3A) revealed striking within-group uniformity; animals receiving the same intervention clustered together taxonomically, while clear separation emerged between the AZM cohort and both CEC-treated and control animals. Aggregate group comparisons (Fig. 3B) confirmed that AZM exposure markedly increased relative abundances of *Adlercreutzia* and *Enterocloster*, coincident with sharp declines in *Akkermansia*. Notably, genus-level compositions in the CEC group remained statistically

indistinguishable from controls, indicating class-specific rather than generalized antibiotic effects. To pinpoint discriminatory taxa, linear discriminant analysis effect size (LEfSe) was applied with a rigorous LDA threshold exceeding 4 (Fig. 3C). Results identified *Enterocloster* and *Flavonifractor* as the strongest genus-level biomarkers enriched in AZM-exposed animals, whereas *Ligilactobacillus* emerged as the predominant discriminatory genus in the control group.

Consistent with observations at the genus level, species-level taxonomic assignment resolved compositional shifts with greater specificity. Relative abundance distributions for the 20 most prevalent bacterial species in individual samples (Fig. 4A) again demonstrated robust within-group consistency and pronounced divergence between the AZM group and the CEC/control cohorts. Group-level species abundance analysis (Fig. 4B) revealed that AZM exposure was associated with a significant increase in the relative abundance of *Adlercreutzia equolifaciens* and *Enterocloster bolteae*, alongside a marked depletion of the beneficial commensal *Akkermansia muciniphila*. Conversely, the CEC and Control groups exhibited consistently high abundances of *Akkermansia muciniphila* and *Parabacteroides goldsteinii*, with no significant difference between the CEC and Control groups. LEfSe analysis with an LDA score threshold of > 4 (Fig. 4C) further identified *Enterocloster bolteae* and *Flavonifractor plautii* as the key species-level discriminatory biomarkers enriched in AZM-exposed mice, contrasting with the significant enrichment of *Ligilactobacillus murinus* and *Escherichia coli* in the control group.

3.3 Functional Analysis of the Gut Microbiome

Beyond compositional changes, antibiotic exposure significantly reshaped the functional potential of the microbiome. To compare the functional bacteria genes, we compared gut microbial functions across these groups. The enriched KEGG pathways encompassed metabolism, genetic information processing, human diseases, cellular processes, organismal systems, and environmental information processing (Fig. 5A). **T**he AZM microbiome was enriched for amino acid metabolism and membrane transport, while the Control group prioritized cofactor/vitamin metabolism. (Fig. 5B).

The MetaCyc database (https://metacyc.org) is used to predict the functions of bacterial metabolic pathways among these groups. 56 bacterial MetaCyc pathways with statistically richer levels in AZM samples included glycogen biosynthesis I (from ADP-D-Glucose), sucrose biosynthesis II, purine ribonucleosides degradation, adenine and adenosine salvage III, and L-arginine biosynthesis I (via L-ornithine). Notably, the upregulation of glycogen metabolism pathways aligns with previous findings linking altered adipose tissue glycogen enzymes to obesity [25]. 35 bacterial MetaCyc pathways with statistically richer levels in CEC samples included inosine-5'-phosphate biosynthesis I, inosine-5'-phosphate biosynthesis II, preQ0 biosynthesis, cis-vaccenate biosynthesis, and glycolysis II (from fructose 6-phosphate). And 96 bacterial MetaCyc pathways with statistically richer levels in control samples included L-arginine biosynthesis IV (archaea), gluconeogenesis III, isoprene biosynthesis I, methylerythritol phosphate pathway II, and UDP-N-acetyl-D-glucosamine biosynthesis I (Fig. 5C).

3.4 Metabolomics Changes in Response to Antibiotic Treatment

Untargeted metabolomic profiling was conducted on the same fecal specimens analyzed by metagenomic sequencing to investigate potential links between microbial community shifts and metabolic output. Multivariate statistical modeling using Partial Least Squares Discriminant Analysis (PLS-DA) and Orthogonal Partial Least Squares Discriminant Analysis (OPLS-DA) yielded clear separation of samples by treatment group (Figs. 6A and 6B), reinforcing the presence of group-specific metabolic signatures.

Visual inspection of the hierarchical clustering heatmap displaying the 30 most differentially abundant metabolites (Fig. 6C) revealed distinct accumulation patterns associated with each antibiotic regimen. Relative to controls, the AZM group showed elevated levels of the lignan eudesmin, the amino acid L-methionine, the fatty acid derivative cis-9,10-epoxystearic acid, the sphingolipid hexadecasphinganine, and L-norleucine. In contrast, CEC-treated animals exhibited enrichment of a different metabolite set, including the sesquiterpenoid tashironin, aromatic amino acids L-phenylalanine and L-tryptophan, the tryptophan catabolite indolelactic acid, the lignan magnoshinin, the aldosterone antagonist eplerenone, linoleic acid amide, L-rhamnonate, the vitamin E metabolite D-alpha-tocopherylquinone, and the fatty acid primary amide oleamide. Metabolites more abundant specifically in control animals included the phospholipid 1-palmitoyl-sn-glycero-3-phosphocholine, the dipeptides L-leucyl-L-valine and L-isoleucyl-L-proline, the branched-chain amino acid L-isoleucine, and the acetate derivative 1,2-dihydroxyheptadec-16-en-4-yl acetate. These metabolomic profiles aligned with the treatment-specific grouping observed in multivariate analys**es.**

3.5 Metabolomics Enrichment Analysis

Although we could identify the metabolic pathways with significant differences among various groups (t-test, $P < 0.05$) through ORA enrichment analysis, we still did not know whether these metabolites play a key role in these metabolic pathways. Therefore, we calculated the significance of the metabolites under focus in the metabolic pathways (measured by Impact) through topological analysis. Combining topological analysis with ORA enrichment analysis could determine whether a metabolic pathway plays a key role in the studied biological process. Because there was a significant difference in weight between the AZM and Control groups, we would focus on the differential metabolites between these two groups. From our study, we could know that arginine biosynthesis, sphingolipid metabolism, 2-oxocarboxylic acid metabolism, and steroid hormone biosynthesis were the enriched metabolic pathways (Fig. 6D). Several metabolic pathways were differentially enriched between the AZM and Control groups. Within 2-oxocarboxylic acid metabolism, N-acetylornithine (elevated in controls) and L-ornithine (elevated in the AZM group) emerged as central metabolites. Arginine biosynthesis involved L-glutamine (higher in AZM), N-acetylornithine (higher in controls), and L-ornithine. In sphingolipid metabolism, sphingosine, sphinganine, and phytosphingosine were all elevated in controls. Additionally,

steroid hormone biosynthesis was differentially regulated, with 11β-hydroxyprogesterone, estriol, and estrone 3-sulfate enriched in controls, whereas adrenosterone was enriched in the AZM group.

3.6 Integrative Correlation Analyses between Gut Microbiome and Metabolome Data

To explore the potential interactions between the gut microbiome changes and metabolic products, a correlation matrix was generated using Spearman correlation. From the heatmaps (Fig. 7A and 7B), we could see different microbial groups and unique association patterns with different metabolites, and these patterns include both promoting positive correlation and negative correlation. This indicated that the gut microbiota played diverse roles in the body by producing or consuming different metabolites.

From the barplot (Fig. 7C), we found that *Bacteroidia* and *Verrucomicrobiae* were the positively correlated microbiota. When the abundance of these groups increased, the abundance of microbiota in the graph was likely to increase as well. On the contrary, the remaining microorganisms in the figure were negatively correlated microbial groups. Their regulation of metabolites may have a negative effect. And we found some functions that promoted the production of metabolites, and there were also some functions that inhibited the production of metabolites (Fig. 7D).

3.7 Correlations between Gut Microbiota and Metabolic Changes

Microbially derived metabolites influenced the host through multiple pathways. Recent evidence showed that certain metabolic products of gut microbiota could enter the bloodstream and exert important influences on the physiology and behavior of the hosts [26]. Thus, we further explored the relationship between microbiota and metabolites with a correlation matrix using Spearman correlation (Fig. 8A). The abundance of most species, such as *Bacteroidia*, *Verrucomicrobiae*, and *Gammaproteobacteria*, was positively correlated with the level of lysoPE, baccatin, theophylline, 4-methylcatechol, N-acetyltaurine, and tenovin-6. On the contrary, the abundance of *Clostridia*, *Epsilonproteobacteria*, *Spirochaetia*, and *Alphaproteobacteria* was negatively correlated with the level of these metabolites. What deserves our attention was that *Bacteroidia* and *Clostridia* were both closely related to the formation of SCFA. They exhibited opposing correlations with host metabolites in this context, suggesting distinct functional roles within the metabolic network.

4. Discussion

Numerous previous studies have demonstrated that antibiotic-induced disruption of the gut microbiota in early life is associated with an increased risk of childhood obesity [9, 27]. However, the mechanisms underlying this association and the differential effects of specific antibiotic classes have not been fully characterized.

Given the rising prevalence of childhood obesity, further studies specifically designed to evaluate the relationship between antibiotics and obesity are urgently needed. In this exploratory study, we provide a comparative multi-omics analysis demonstrating that early-life exposure to a high dose of azithromycin (AZM), but not a standard dose of cefaclor (CEC), is associated with significant alterations in the gut microbiota-metabolome axis and increased body weight gain in juvenile mice. These findings generate the hypothesis that macrolide antibiotics may pose a distinct risk for metabolic changes compared to other classes, a premise that requires rigorous validation in pharmacologically controlled and causally designed studies.

AZM treatment induced marked shifts in the relative abundances of several bacterial species with established links to metabolic health. Enrichment of *Adlercreutzia equolifaciens* and *Enterocloster bolteae* accompanied depletion of *Akkermansia muciniphila* and *Ligilactobacillus murinus* in azithromycin-exposed animals. These compositional changes mirror patterns reported elsewhere in the literature. For *A. equolifaciens*, positive correlations with BMI emerged both in a longitudinal obese cohort [28] and in metagenomic data from a northern Netherlands population [29]; our observation of elevated *A. equolifaciens* in the AZM group aligns with those reports. Regarding *E. bolteae*, prior work links this species to elevated urate concentrations and enhanced short-chain fatty acid production [30], with increased abundances documented in type 2 diabetes patients relative to healthy controls [31] and in individuals with non-alcoholic steatohepatitis [32, 33]. The expansion of *E. bolteae* in our AZM-treated mice thus parallels its reported enrichment in metabolically compromised human populations. Conversely, taxa depleted following AZM exposure have been associated with protective metabolic effects. *Akkermansia muciniphila* is widely recognized for its probiotic potential [34, 35]; multiple metagenomic surveys describe inverse relationships between its abundance and metabolic disorders, including obesity and diabetes [36, 37]. Experimental studies further demonstrate that *A. muciniphila* administration attenuates diabetes and obesity progression in murine models [38, 39]. Our finding of reduced *A. muciniphila* in AZM-treated animals is consistent with this protective paradigm. Similarly, *Parabacteroides goldsteinii* exhibits anti-obesogenic properties; oral administration to high-fat diet-fed mice reduces adiposity while promoting adipose tissue thermogenesis, strengthening intestinal barrier function, and attenuating inflammatory markers and insulin resistance [40, 41]. Although *P. goldsteinii* abundances did not differ significantly between treatment groups in our dataset, its prominence in control animals aligns with its described beneficial profile. *Ligilactobacillus murinus*, another commensal depleted by AZM, correlates positively with intestinal health measures and holds recognized probiotic potential [42].

An increasing number of studies have shown that the intestinal microbiota can synthesize and degrade amino acids [43]. Furthermore, changes in the intestinal microbial community and branched-chain amino acid levels are closely related to obesity and insulin resistance [44]. In our study, after azithromycin intervention, the differential intestinal microbiota was enriched in the amino acid metabolism pathway. Furthermore, through non-target metabolic analysis, we discovered that after the intervention with antibiotics, the levels of various amino acids and their derivatives had changed. Takeshi et al. discovered that branched-chain amino acid supplementation was often beneficial to energy expenditure [45].

However, increased circulating levels of BCAA are linked to obesity and diabetes. The mechanisms of this paradox remain unclear. And in our study, we found that the reduction of branched-chain amino acids in fecal metabolites was associated with obesity. Tryptophan metabolism played a significant role in obesity. Its metabolites affect the metabolic health through various pathways [46]. Through this study, we found that the level of 5-methoxy-L-tryptophan in fecal metabolites was negatively correlated with obesity. Wang et al. found a reduction in adipocyte uptake of methionine [47]. This was consistent with the result we found in our study, which was that the content of methionine in the fecal metabolites of the AZM group increased.

Most obese people had lipid metabolism disorders. Soyasapogenol B exerted an anti-obesity effect on adipocytes by lowering the cellular triglyceride level by accelerating triglyceride lipolysis with reduced resistin secretion [48]. However, our research found that Soyasapogenol B was positively correlated with obesity. Anita et al. found dietary linoleic acid induced obesity [49]. And we found that, as the amide product of linoleic acid, linoleic acid amide was positively correlated with the weight gain of mice. Disorders in bile acid metabolism caused obesity [50]. The dysbiosis of the microbiota in obese patients may affect the types and quantities of bile acids [51]. Our research also found that antibiotics affected the level of bile acid derivatives. *Akkermansia muciniphila* was a beneficial gut commensal and could alleviate high-fat-diet-related metabolic-associated fatty liver disease by modulating gut microbiota and bile acids [52].

The differential effects of AZM and CEC on the gut microbiota are consistent with their distinct antimicrobial spectra. As a macrolide antibiotic, AZM primarily targets Gram-positive bacteria by binding to the 50S ribosomal subunit, while CEC, a second-generation cephalosporin, predominantly targets Gram-negative bacteria via inhibition of cell wall synthesis. The observed expansion of Gram-positive taxa (Adlercreutzia, Enterocloster) and depletion of the Gram-negative Akkermansia muciniphila in the AZM group aligns with AZM's spectrum, although the incomplete suppression of certain Gram-positive anaerobes suggests differential susceptibility within this group. In contrast, the lack of significant weight gain and microbiota disruption in the CEC group may reflect its narrower spectrum or lower tested dose. These pharmacological distinctions should be considered when interpreting the class-specific metabolic risks of pediatric antibiotic exposure.

Several limitations should be acknowledged. First, and most importantly, the doses of AZM (100 mg/kg) and CEC (20 mg/kg) were not pharmacokinetically equivalent. Therefore, the observed differential effects cannot be solely attributed to the antibiotic class, as they may be driven by the disparity in dose. Future comparative studies must employ doses that achieve equivalent therapeutic exposures in the murine model. Second, we measured only total body weight gain, not body composition. Consequently, we cannot conclude that the weight gain reflects increased adiposity; it may be due to other factors. Third, the study is entirely associative. We have not demonstrated that the microbiota changes cause the weight gain; this would require fecal microbiota transplantation experiments. Fourth, the use of only male mice limits the generalizability of our findings. Finally, the lack of systemic metabolic markers (e.g., glucose, insulin, leptin) prevents us from linking the gut-level changes to host metabolic health. This

study should therefore be viewed as a hypothesis-generating investigation that identifies strong correlations, which must be confirmed and extended in more rigorously designed studies.

Conclusion

In this exploratory study, we show that early-life exposure to a high dose of AZM, but not a standard dose of CEC, is significantly associated with increased body weight gain, alongside distinct alterations in the gut microbiota and fecal metabolome in juvenile mice. AZM treatment correlated with an enrichment of specific bacterial taxa and perturbations in amino acid and lipid metabolism pathways. These findings generate the hypothesis that azithromycin may pose a class-specific metabolic risk. This work provides a foundation of testable hypotheses for future studies employing pharmacokinetically equivalent dosing, causal validation via FMT, and comprehensive metabolic phenotyping to definitively establish the mechanisms linking specific antibiotic classes to pediatric metabolic health.

Declarations

Ethics Statement

This study was approved by the Animal Care and Use Committee of The First Hospital of Jiaxing, Affiliated Hospital of Jiaxing University (approval number: JXYY2023-027). All animal experiments were conducted in accordance with relevant institutional and national guidelines for the care and use of laboratory animals. At the end of the study, all C57BL/6J mice were anesthetized with isoflurane (3–5% for induction and 1.5–2% for maintenance) in an induction chamber. After deep anesthesia was confirmed by the loss of the pedal withdrawal reflex, the mice were humanely euthanized by cervical dislocation.

Consent to participate

Not applicable.

Consent to publish

Not applicable.

Declaration of Competing Interests

LG is affiliated with AigenX Biosciences Co., Ltd. The authors declare that this affiliation does not constitute a competing interest.

Funding

This project was supported by the Scientific Research Fund of Zhejiang Provincial Education Department (33323166AL)

Data availability

The fecal shotgun metagenomic sequencing datasets generated and/or analysed during the current study are available in the NCBI Sequence Read Archive repository under BioProject accession number PRJNA1457376: https://www.ncbi.nlm.nih.gov/bioproject/PRJNA1457376. The fecal untargeted metabolomics datasets generated and/or analysed during the current study are available from the corresponding author upon reasonable request.

Author Contributions Statement

Yuhui Yao : Conceptualization, designed project and writing; Shanshan Zhan: Conceptualization and methodology; animal experiments; Jinhua Hu , Lei Yang: Data curation and formal analysis; prepared figures; Liang Guo and Shunfeng Mao: Conceived and designed project; Project administration and supervision. All authors have read and agreed to the published version of the manuscript.

References

1. Jebeile H, et al. *Obesity in children and adolescents: epidemiology, causes, assessment, and management.* The Lancet. Diabetes Endocrinol. 2022;10(5):351–65.
2. Horesh A, et al. Adolescent and Childhood Obesity and Excess Morbidity and Mortality in Young Adulthood-a Systematic Review. Curr Obes Rep. 2021;10(3):301–10.
3. Jebeile H, et al. Addressing psychosocial health in the treatment and care of adolescents with obesity. Obes (Silver Spring Md). 2021;29(9):1413–22.
4. Trasande L et al. *Infant antibiotic exposures and early-life body mass.* International Journal of Obesity (2005), 2012. 37(1): pp. 16–23.
5. Bailey LC, et al. Association of antibiotics in infancy with early childhood obesity. JAMA Pediatr. 2014;168(11):1063–9.
6. Ray K. Gut microbiota: Adding weight to the microbiota's role in obesity–exposure to antibiotics early in life can lead to increased adiposity. Nat Rev Gastroenterol Hepatol. 2012;9(11):615.
7. Cerdó T et al. The Role of Probiotics and Prebiotics in the Prevention and Treatment of Obesity. Nutrients, 2019. 11(3).
8. Lee CJ, Sears CL, Maruthur N. Gut microbiome and its role in obesity and insulin resistance. Volume 1461. Annals of the New York Academy of Sciences; 2020. pp. 37–52. 1.
9. Principi N, Esposito S. Antibiotic administration and the development of obesity in children. Int J Antimicrob Agents. 2016;47(3):171–7.
10. Gaskins HR, Collier CT, Anderson DB. Antibiotics as growth promotants: mode of action. Animal Biotechnol. 2002;13(1):29–42.
11. Kechin A, et al. cutPrimers: A New Tool for Accurate Cutting of Primers from Reads of Targeted Next Generation Sequencing. J Comput Biology: J Comput Mol Cell Biology. 2017;24(11):1138–43.

12. Schmieder R, Edwards R. Quality control and preprocessing of metagenomic datasets. Bioinf (Oxford England). 2011;27(6):863–4.
13. Langmead B, Salzberg SL. Fast gapped-read alignment with Bowtie 2. Nat Methods. 2012;9(4):357–9.
14. Wood DE, Salzberg SL. Kraken: ultrafast metagenomic sequence classification using exact alignments. Genome Biol. 2014;15(3):R46.
15. Lu J et al. Bracken: estimating species abundance in metagenomics data. PeerJ Comput Sci, 2017. 3.
16. Mandal S, et al. Analysis of composition of microbiomes: a novel method for studying microbial composition. Microb Ecol Health Disease. 2015;26:27663.
17. Brum JR, et al. Ocean plankton. Patterns and ecological drivers of ocean viral communities. Volume 348. New York, N.Y.): Science; 2015. p. 1261498. 6237.
18. Segata N, et al. Metagenomic biomarker discovery and explanation. Genome Biol. 2011;12(6):R60.
19. Zhu W, Lomsadze A, Borodovsky M. Ab initio gene identification in metagenomic sequences. Nucleic Acids Res. 2010;38(12):e132.
20. Kim J, et al. FMAP: Functional Mapping and Analysis Pipeline for metagenomics and metatranscriptomics studies. BMC Bioinformatics. 2016;17(1):420.
21. Franzosa EA, et al. Species-level functional profiling of metagenomes and metatranscriptomes. Nat Methods. 2018;15(11):962–8.
22. Villar E, et al. Ocean plankton. Environmental characteristics of Agulhas rings affect interocean plankton transport. Volume 348. New York, N.Y.): Science; 2015. p. 1261447. 6237.
23. Buchfink B, Xie C, Huson DH. Fast and sensitive protein alignment using DIAMOND. Nat Methods. 2014;12(1):59–60.
24. Want EJ, et al. Global metabolic profiling of animal and human tissues via UPLC-MS. Nat Protoc. 2012;8(1):17–32.
25. Lu B, et al. Metabolic crosstalk: molecular links between glycogen and lipid metabolism in obesity. Diabetes. 2014;63(9):2935–48.
26. Sarkar A, et al. Psychobiotics and the Manipulation of Bacteria-Gut-Brain Signals. Trends Neurosci. 2016;39(11):763–81.
27. Gérard P. Gut microbiota and obesity. Cell Mol Life Sci. 2015;73(1):147–62.
28. Deng K, et al. Temporal relationship among adiposity, gut microbiota, and insulin resistance in a longitudinal human cohort. BMC Med. 2022;20(1):171.
29. Chen L et al. The long-term genetic stability and individual specificity of the human gut microbiome. Cell, 2021. 184(9).
30. Bunt D, et al. Gut microbiota-mediated conversion of mangiferin to norathyriol alters short chain fatty acid and urate metabolism. Gut Microbes. 2025;17(1):2508422.

31. Park S, Zhang T, Kang S. Fecal Microbiota Composition, Their Interactions, and Metagenome Function in US Adults with Type 2 Diabetes According to Enterotypes. Int J Mol Sci, 2023. 24(11).
32. Mbaye B, et al. Increased fecal ethanol and enriched ethanol-producing gut bacteria Limosilactobacillus fermentum, Enterocloster bolteae, Mediterraneibacter gnavus and Streptococcus mutans in non-alcoholic steatohepatitis. Front Cell Infect Microbiol. 2023;13:1279354.
33. Ruuskanen MO et al. Links between gut microbiome composition and fatty liver disease in a large population sample. Gut Microbes, 2021. 13(1).
34. Zhai Q, et al. A next generation probiotic, Akkermansia muciniphila. Crit Rev Food Sci Nutr. 2018;59(19):3227–36.
35. Cani PD, et al. Akkermansia muciniphila: paradigm for next-generation beneficial microorganisms. Nat Rev Gastroenterol Hepatol. 2022;19(10):625–37.
36. Reunanen J, et al. Akkermansia muciniphila Adheres to Enterocytes and Strengthens the Integrity of the Epithelial Cell Layer. Appl Environ Microbiol. 2015;81(11):3655–62.
37. Yassour M, et al. Sub-clinical detection of gut microbial biomarkers of obesity and type 2 diabetes. Genome Med. 2016;8(1):17.
38. Parks BW, et al. Genetic control of obesity and gut microbiota composition in response to high-fat, high-sucrose diet in mice. Cell Metabol. 2013;17(1):141–52.
39. Suriano F, et al. Novel insights into the genetically obese (ob/ob) and diabetic (db/db) mice: two sides of the same coin. Microbiome. 2021;9(1):147.
40. Wu Y, et al. Unraveling the Obesity-Combating Potential of Parabacteroides goldsteinii and Bacteroides sartorii: A Dual-Probiotic Approach. Probiotics and Antimicrobial Proteins; 2025.
41. Wu T-R, et al. Gut commensal Parabacteroides goldsteinii plays a predominant role in the anti-obesity effects of polysaccharides isolated from Hirsutella sinensis. Gut. 2018;68(2):248–62.
42. Chuandong Z, et al. Distribution and roles of Ligilactobacillus murinus in hosts. Microbiol Res. 2024;282:127648.
43. Pedersen HK, et al. Human gut microbes impact host serum metabolome and insulin sensitivity. Nature. 2016;535(7612):376–81.
44. Ridaura VK, et al. Gut microbiota from twins discordant for obesity modulate metabolism in mice. Volume 341. New York, N.Y.): Science; 2013. p. 1241214. 6150.
45. Yoneshiro T, et al. BCAA catabolism in brown fat controls energy homeostasis through SLC25A44. Nature. 2019;572(7771):614–9.
46. Agus A, Planchais J, Sokol H. Gut Microbiota Regulation of Tryptophan Metabolism in Health and Disease. Volume 23. Cell Host & Microbe; 2018. pp. 716–24. 6.
47. Wang S, et al. PPAR-γ integrates obesity and adipocyte clock through epigenetic regulation of Bmal1. Theranostics. 2022;12(4):1589–606.

48. Iwamoto K, et al. Soyasapogenols reduce cellular triglyceride levels in 3T3-L1 mouse adipocyte cells by accelerating triglyceride lipolysis. Biochem Biophys Rep. 2018;16:44–9.
49. Alvheim AR et al. *Dietary linoleic acid elevates endogenous 2-AG and anandamide and induces obesity.* Obesity (Silver Spring, Md.), 2012. 20(10): pp. 1984–1994.
50. Chiang JYL. Bile acid metabolism and signaling. Compr Physiol. 2013;3(3):1191–212.
51. Mouzaki M, et al. Bile Acids and Dysbiosis in Non-Alcoholic Fatty Liver Disease. PLoS ONE. 2016;11(5):e0151829.
52. Wu W, et al. Akkermansia muciniphila alleviates high-fat-diet-related metabolic-associated fatty liver disease by modulating gut microbiota and bile acids. Microb Biotechnol. 2023;16(10):1924–39.

Figures

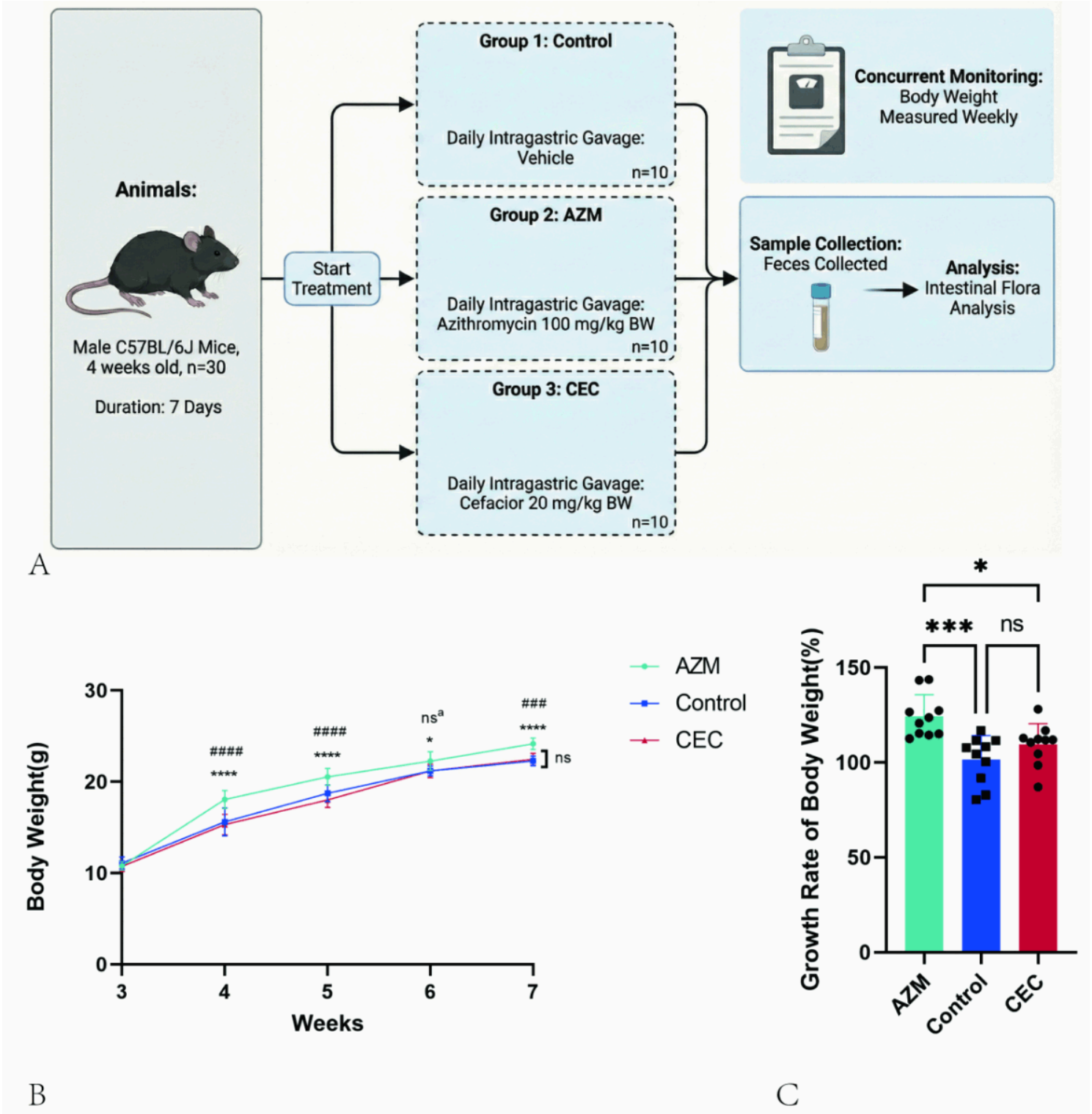


Figure 1

The impact of long-term use of antibiotics on the body weight of juvenile mice. (A) The schedule for the experiment and various treatments for each group of mice. (B) The body weight changes of various groups **over** 4 weeks. (C) Growth Rate of Body Weight. *P < 0.05, ****P < 0.0001, *Comparison, AZM versus control. $^{\#}P$ < 0.05, $^{\#\#\#}P$ < 0.001, $^{\#\#\#\#}P$ < 0.0001, ns: P>0.05, $^{\#}$Comparison, AZM versus CEC. Data were analyzed by one-way ANOVA followed by Tukey's post-hoc test.

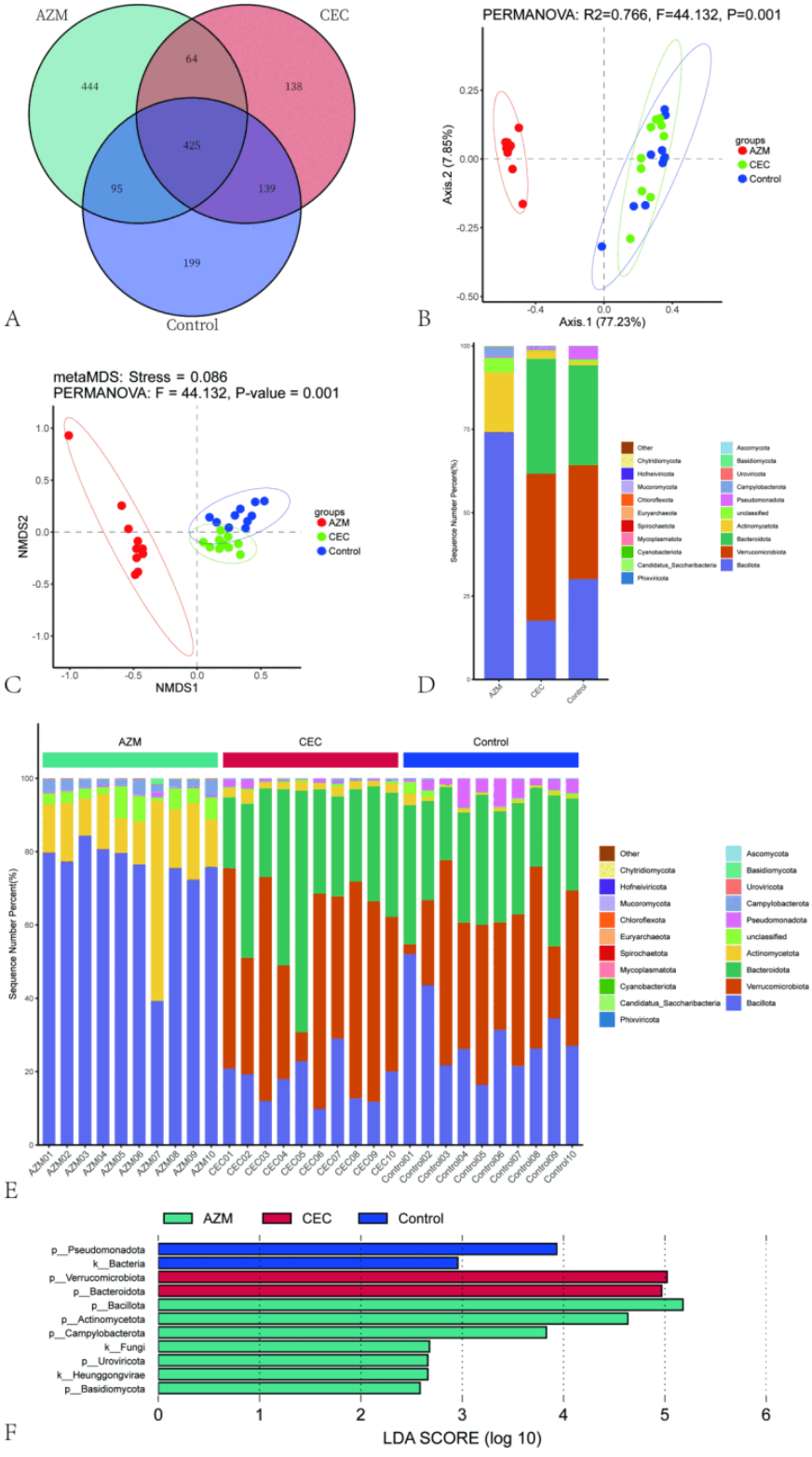


Figure 2

Long-term Exposure to Antibiotics Alters Intestinal Microbiota Composition and Structure. (A) Venn diagram showing unique and shared annotated bacterial species among the AZM, CEC, and control groups. (B) Principal Coordinates Analysis (PCoA) based on Bray-Curtis distance among the AZM, CEC, and Control groups. PERMANOVA was performed using Bray-Curtis distance with 999 permutations (R^2=0.766, *P*=0.001). (C) Non-Metric Multi-Dimensional Scaling (NMDS) of the AZM, CEC, and control

groups. PERMANOVA, F = 44.132, *P* = 0.001. (D) The relative abundance of gut microbiota in each group at the phylum level. (E) The relative abundance of gut microbiota in each sample at **the** phylum level. (F) Linear discriminant analysis effect size (LEfSe) scores for bacterial taxa differentially abundant among the AZM, CEC, and Control groups (LDA>2).

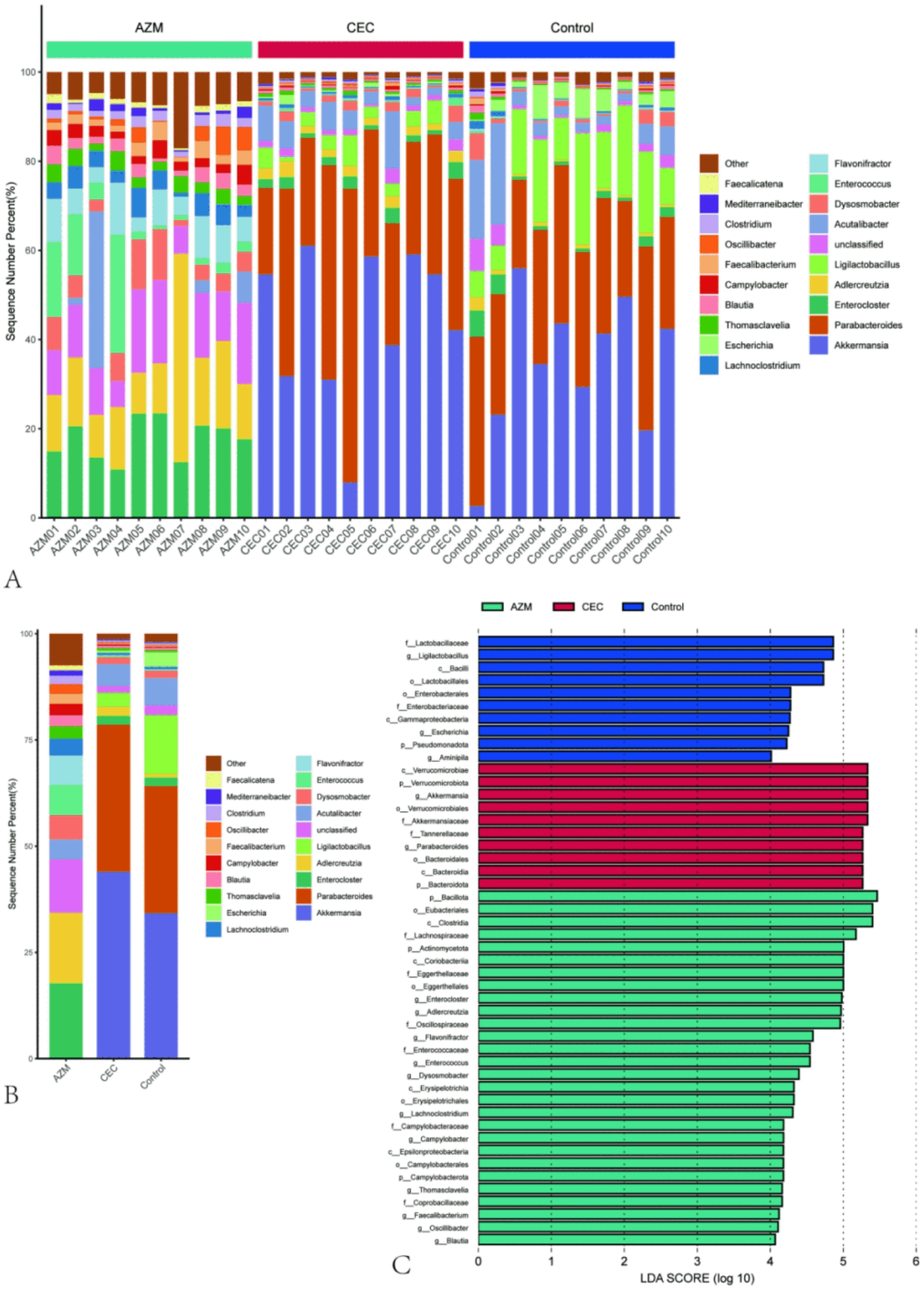


Figure 3

Long-term Exposure to Antibiotics Alters Intestinal Microbiota Composition and Structure at the Genus Level. (A) The relative abundance of gut microbiota in each sample at **the** genus level. (B) The relative abundance of gut microbiota in each group at the genus level. (C) Linear discriminant analysis effect size (LEfSe) scores for bacterial taxa differentially abundant among the AZM, CEC, and control groups (LDA>4).

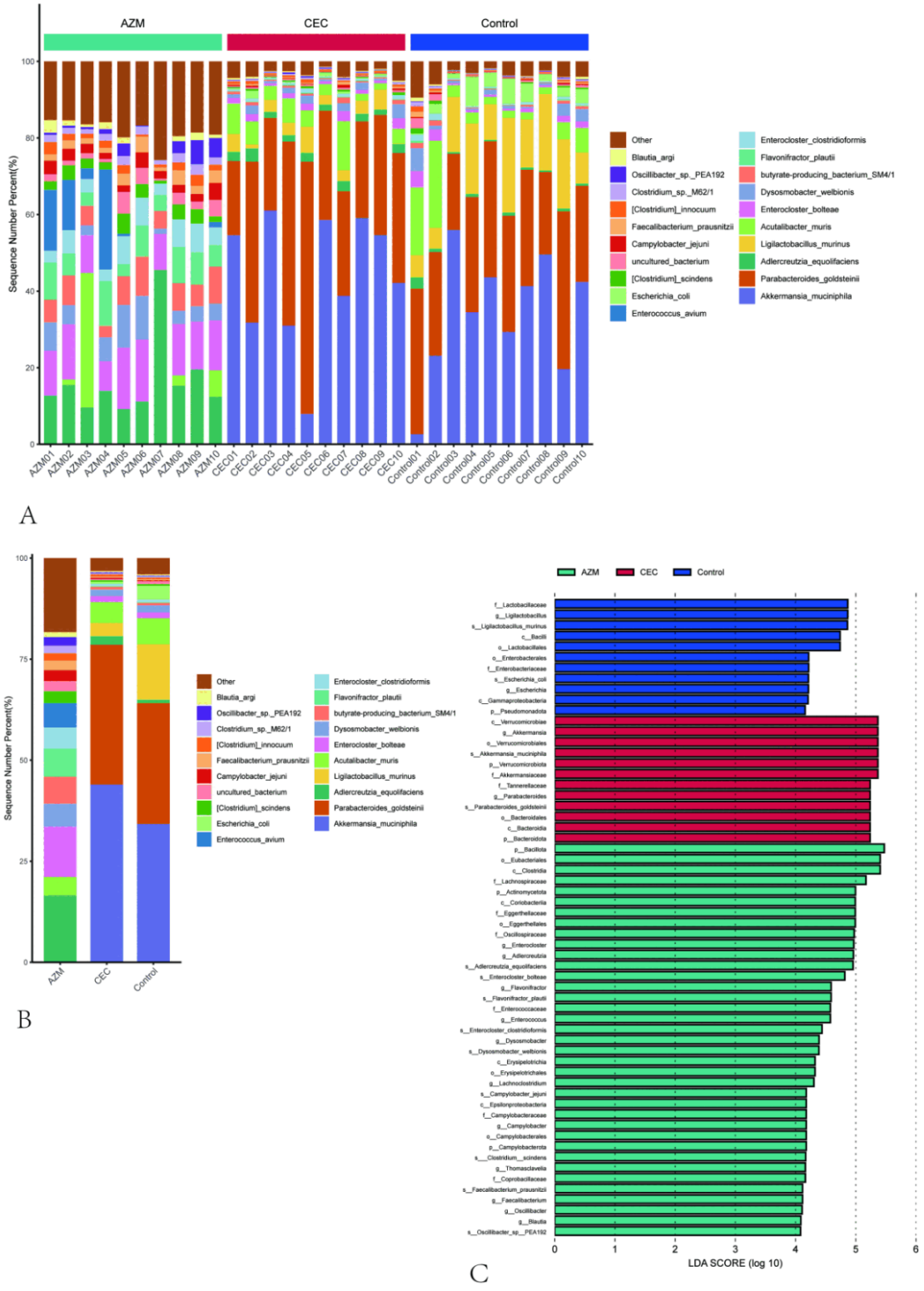


Figure 4

Long-term Exposure to Antibiotics Alters Intestinal Microbiota Composition and Structure at the Species Level. (A) The relative abundance of gut microbiota in each sample at the species level. (B) The relative abundance of gut microbiota in each group at the species level. (C) Linear discriminant analysis effect size (LEfSe) scores for bacterial taxa differentially abundant among the AZM, CEC, and Control groups (LDA>4).

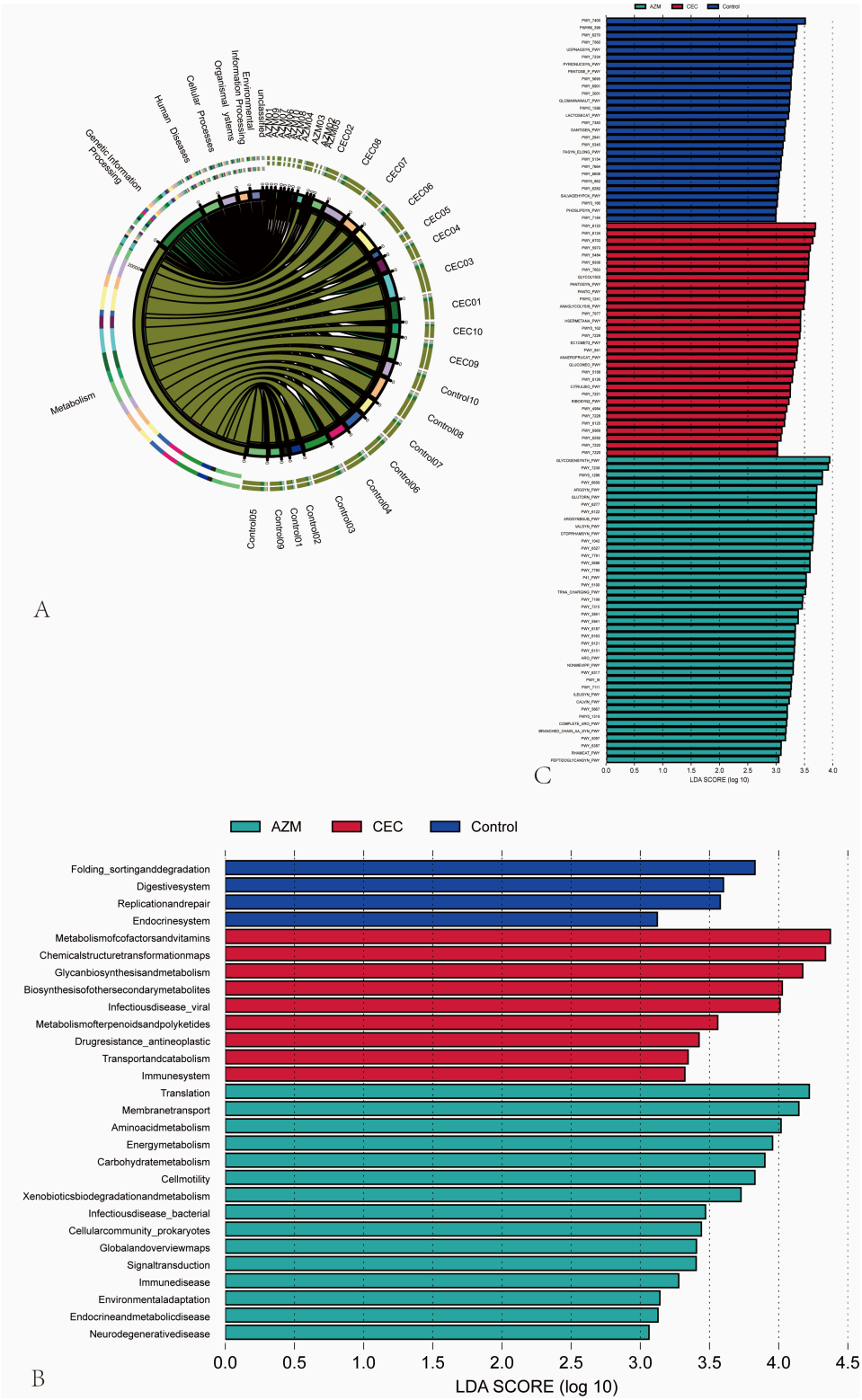


Figure 5

Functional Analysis of the Intestinal Microbiota. (A) Significant KEGG pathways of differentially **abundant**bacterial taxa among the AZM, CEC, and Control groups. (B) Linear discriminant analysis effect size (LEfSe) scores for KEGG functions of bacterial taxa differentially abundant among the AZM, CEC, and Control groups (LDA>4). (C) Linear discriminant analysis effect size (LEfSe) scores for MetaCyc pathways of bacterial taxa differentially abundant among the AZM, CEC, and Control groups (LDA>3).

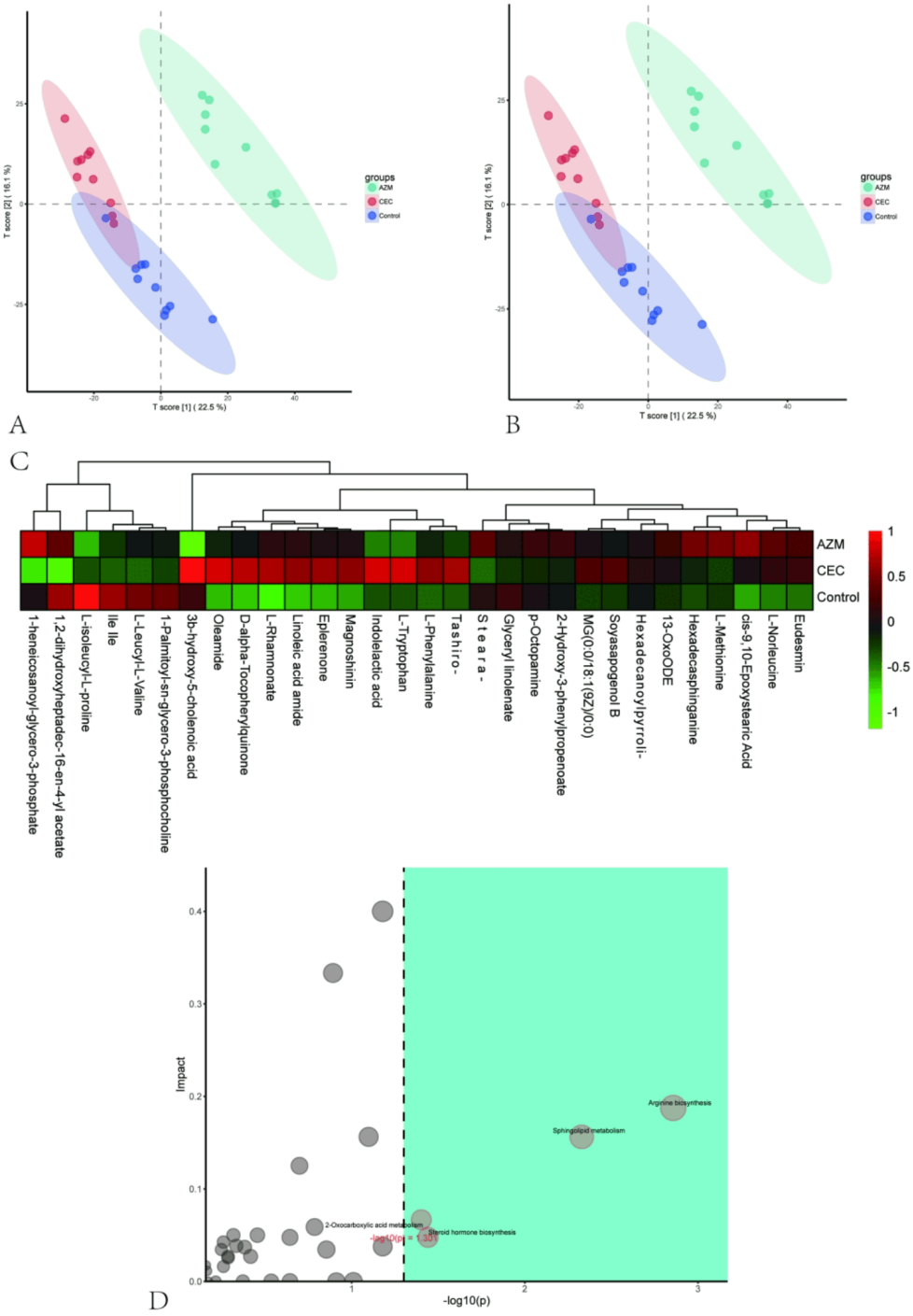


Figure 6

Metabolomics Changes in Response to Antibiotic Treatment. (A) **T**he clustering analyses of partial least-squares discriminant analysis (PLS-DA). (B) The orthogonal partial least-squares discriminant analysis (OPLS-DA). (C) Heatmap of the top 30 ranked significantly different metabolites among the AZM, CEC, and Control groups. The correlation effect is indicated by a color gradient from green (negative correlation) to red (positive correlation). (D) The over-representation analysis (ORA) of differential metabolites between the AZM and control groups.

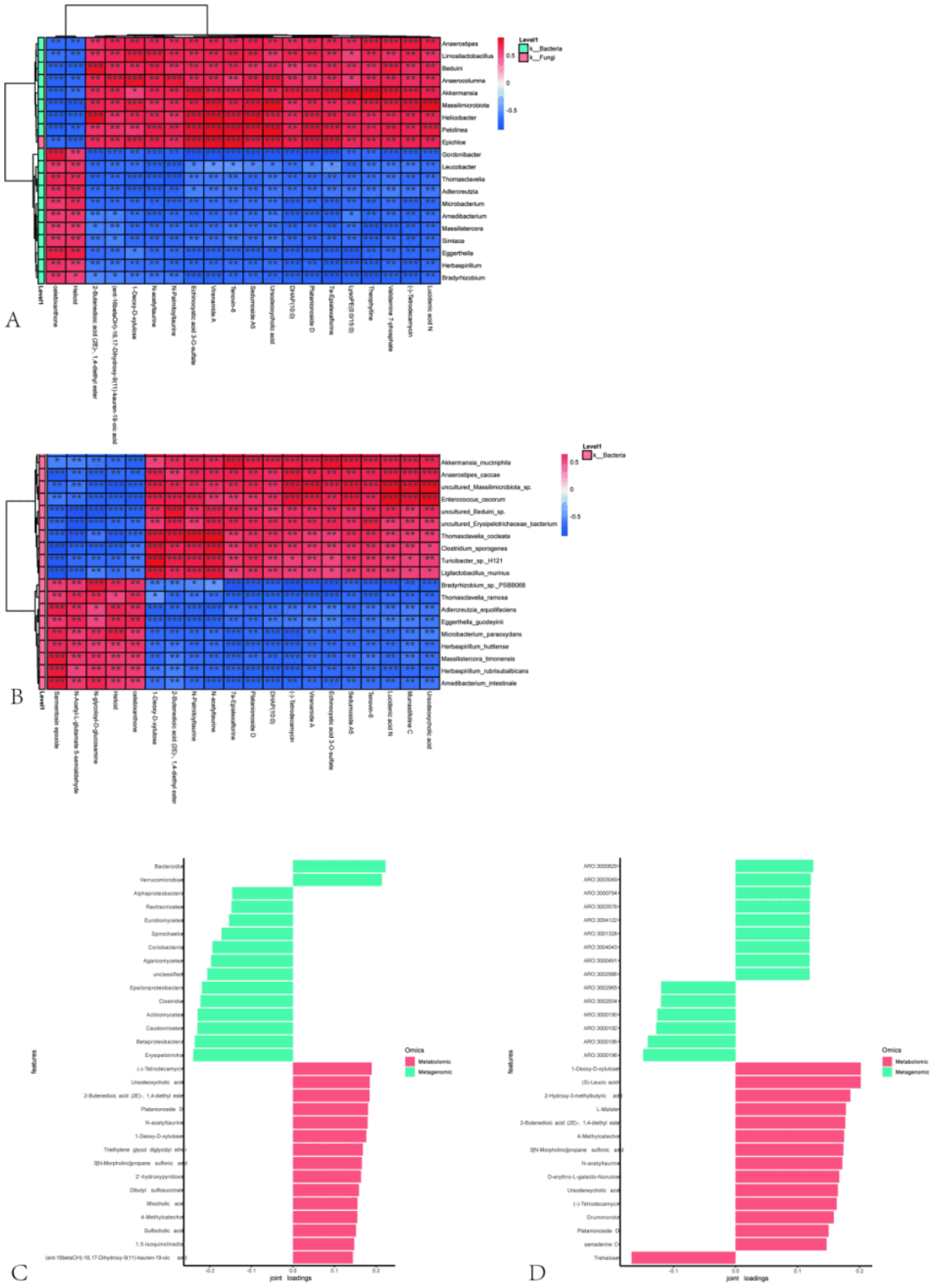


Figure 7

Integrative Correlation Analyses between Gut Microbiome and Metabolome Data. Spearman correlation heatmaps between the gut microbiota and metabolites. (A) Correlation analysis at the genus level. (B) Correlation analysis at the species level. (C) Ranked loading values for species annotations and metabolites. *P < 0.05, **P < 0.01, ***P < 0.001. (D) Ranked loading values for functional annotations and metabolites. The x-axis represents the joint loading values.

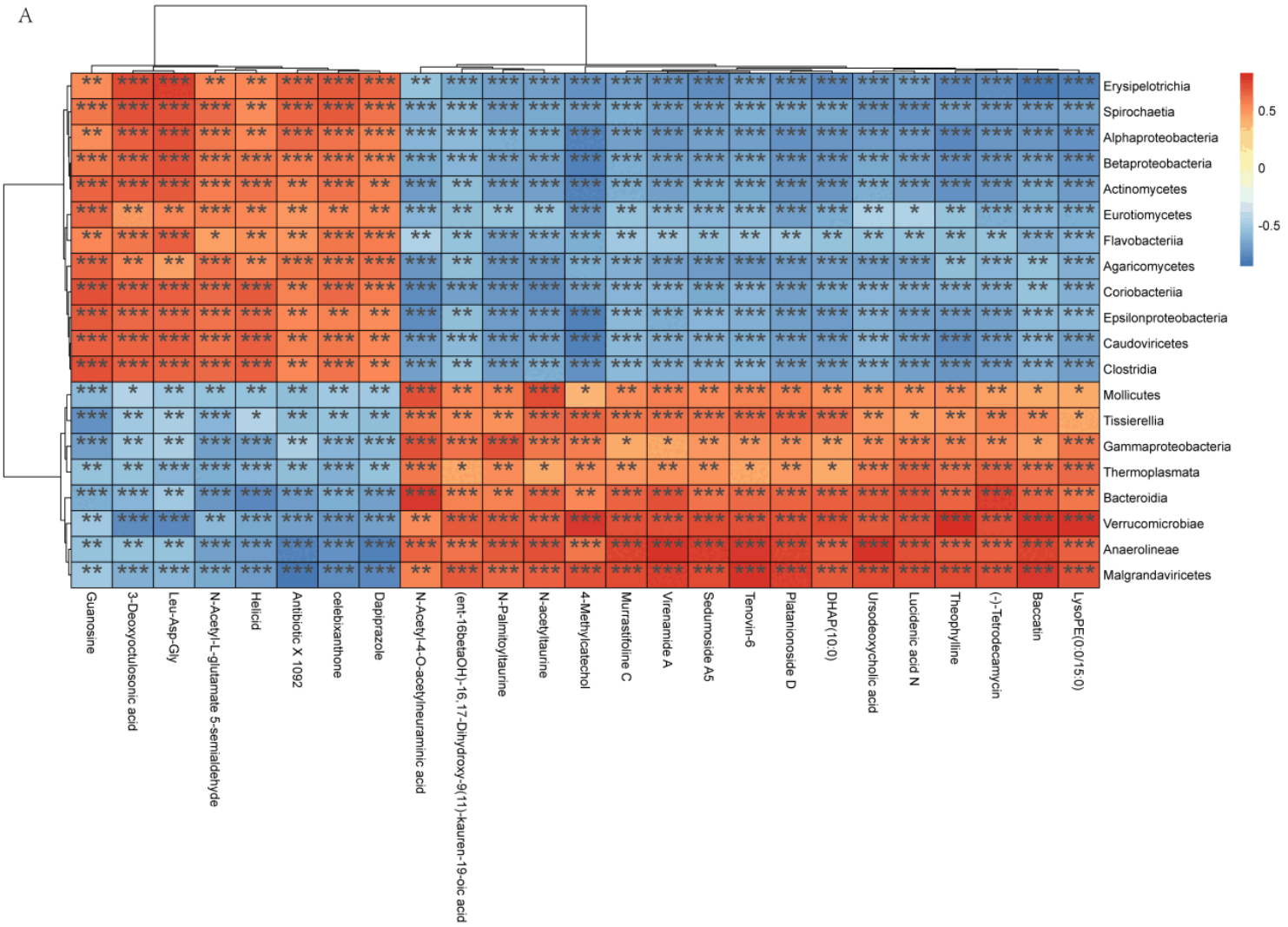


Figure 8

Correlations between Gut Microbiota, Metabolites, and Metabolic Changes. (A) The heatmap illustrates the associations between gut microbial taxa (rows) and differential metabolites (columns). The color gradient represents the Spearman correlation coefficient, with red indicating a positive correlation and blue indicating a negative correlation. *P < 0.05, **P < 0.01, and ***P < 0.001.